Hydride Exchange Reaction in Trimetallic Clusters. An *ab Initio* Molecular Orbital Study of $M_3(CO)_9(\mu\text{-}H)_3(\mu_3\text{-}CH)$ (M = Os, Ru)

Jean-Frédéric Riehl,[†] Nobuaki Koga,[†,§] and Keiji Morokuma*[,†,‡]

Contribution from the Institute for Molecular Science, Myodaiji, Okazaki 444, Japan, School of Informatics and Sciences and Graduate School of Human Informatics, Nagoya University, Nagoya 464-01, Japan, and Cherry L. Emerson Center for Scientific Computation and Department of Chemistry, Emory University, Atlanta, Georgia 30322

Received January 12, 1994. Revised Manuscript Received March 24, 1994[●]

Abstract: An *ab initio* molecular orbital study is presented on the mechanism of the hydride exchange reaction in the trimetallic complex $M_3(CO)_9(\mu\text{-}H)_3(\mu_3\text{-}CH)$ (M = Os, Ru). Based on the calculated structures and energies of many intermediates and transition states, it is proposed that the hydride exchange reaction takes place in multiple steps via two energetically competitive pathways. The "inner" pathway consists of the following steps: (1) migration of the bridging hydride H* to the nearby equatorial terminal position to form a seven-coordinated M; (2) clockwise turnstile rotation of three carbonyls and H* around this M; (3) insertion of H* into the M–C bond; (4) formation of the H*CH transition-state complex as the midpoint of the degenerate exchange process; and finally the reversal of steps 3, 2, and 1. The "outer" pathway involves the following steps: (1′) migration of the bridging H* to the farther-away equatorial terminal position to form a seven-coordinated M; (2′) anticlockwise turnstile rotation of three carbonyls and H*; and finally a merging with step 3 of the "inner" pathway. Some of the above steps may take place as a concerted single step. The calculated barrier heights are in good agreement with the experimental values and support the experiment in that the reaction of the Ru complex should be easier than that of the Os complex. A direct mechanism without involving seven-coordinated intermediates is unlikely.

Introduction

In the last 15 years, the ability of the second and third row transition metals to form stable polymetallic compounds has opened a wide field of organometallic chemistry. Late transition element clusters, in particular the triruthenium and triosmium carbonyl compounds, have come to play a major role in this development. These compounds, which can be seen as derivatives of the original dodecacarbonyls $Ru_3(CO)_{12}$ and $Os_3(CO)_{12}$ (**1**) whose structures have been known for many years,[1] are involved as homogeneous catalysts in many reactions, such as the activation of the C–H bond of dienes and trienes and the insertion of carbonyl.[2] This variety of reactions is attributed to the strength of the metal–metal bonds, which allows various coordination modes like $\mu_2{:}\eta^1$, $\mu_2{:}\eta^2$, $\mu_3{:}\eta^1$, $\mu_3{:}\eta^2$, and $\mu_3{:}\eta^3$. First row transition-metal clusters are less reactive because of the propensity of these compounds to form bridged metal–metal bonds in order to compensate for their intrinsic weakness. Recently, these discrete compounds have also been proposed as models for metallic surfaces since the very peculiar $\mu_3{:}\eta^2{:}\eta^2{:}\eta^2$ coordination mode has been obtained for arene clusters.[3]

Starting from the dodecacarbonyl $M_3(CO)_{12}$ (**1**), many reactions take place through the formation of carbonyl polyhydrides, such as $M_3(CO)_{10}(\mu\text{-}H)_2$ and $M_3(CO)_{10}(\mu\text{-}H)(\mu\text{-}L)$ (L = R, CO, ...), as the first step of the catalytic process. Most of them today are structurally well characterized by X-ray or neutron diffraction[4] and are commonly synthesized. Even though these structural studies have been well developed in the last 10 or 15 years, the dynamic properties of such compounds have been the subjects of only recent studies.

It has been noticed in several of these trimetallic carbonyl polyhydrides that a hydrogen atom connected to a metal center, a terminal or bridging hydride, can undergo site exchange with a hydrogen in a ligand. The first such example, which is the center of our study, is the trimetallic nonacarbonyl $M_3(CO)_9(\mu\text{-}H)_3(\mu_3\text{-}CH)$ (M = Fe, Ru, Os) (**2**), in which the exchange between a hydride bridging a metal–metal bond and the methylidyne hydrogen has been observed.[5,6] It has been shown[6] for Os that, even though the exchange is slow at room temperature, it can be observed by spin saturation transfer at temperatures above 80 °C. The experimental activation parameters for this process are $\Delta H^{\ddagger}$ = 24.0 ± 1.7 kcal/mol and $\Delta S^{\ddagger}$ = 2.0 ± 1.8 cal/deg/mol. For Ru, the exchange is evident at lower temperature (34 °C), and experiments suggest that the energetic parameters should be 3–5 kcal/mol lower than those for Os; the experimental $\Delta G^{\ddagger}$ of the reaction measured at 34 °C is 20.6 kcal/mol. The exchange mechanism depicted in Scheme 1 has been proposed for these two compounds. For reasons of clarity, carbonyl oxygen atoms will be omitted from now on in figures and schemes. The exchange should start by a hydride transfer from an M–M bond to an M–C bond, as shown in a in Scheme 1. The second step, b, is an exchange between the terminal and the bridging H atoms of the CH_2 species thus formed. The system

[†] Institute for Molecular Science.
[§] Nagoya University.
[‡] Emory University.
[●] Abstract published in *Advance ACS Abstracts*, May 15, 1994.

(1) (a) $Os_3(CO)_{12}$: Churchill, M. R.; de Boer, B. G. *Inorg. Chem.* **1977**, *16*, 878. (b) $Ru_3(CO)_{12}$: Churchill, M. R.; Hollander, F. J.; Hutchinson, J. P. *Inorg. Chem.* **1977**, *16*, 2655.

(2) See, for instance: *Comprehensive Organometallic Chemistry*; Wilkinson, G., Ed.; Pergamon Press: Oxford, 1982; Vol. 4.

(3) (a) Gallop, M. A.; Gomez-Sal, M. P.; Housecroft, C. E.; Johnson, B. F. G.; Lewis, J.; Owen, S. M.; Raithby, P. R.; Wright, A. H. *J. Am. Chem. Soc.* **1992**, *114*, 2502. (b) Gallup, M. A.; Johnson, B. F. G.; Keeler, J.; Lewis, J.; Dobson, C. M. *J. Am. Chem. Soc.* **1992**, *114*, 2510. (c) Johnson, B. F. G.; Housecroft, C. E.; Gallup, M. A.; Martinelli, M.; Braga, D.; Grepioni, F. *J. Mol. Catal.* **1992**, *74*, 61. (d) Wadephol, H.; Buchner, K.; Pritzkow, H. *Angew. Chem., Int. Ed. Engl.* **1987**, *26*, 1259. (e) Gomez-Sal, M. P.; Johnson, B. F. G.; Lewis, J.; Raithby, P. R.; Wright, A. H. *J. Chem. Soc., Chem. Commun.* **1985**, 1682.

(4) See, for instance: (a) Broach, R. W.; Williams, J. M. *Inorg. Chem.* **1979**, *18*, 314. (b) Churchill, M. R.; Lashewycz, R. A. *Inorg. Chem.* **1979**, *18*, 1926. (c) Churchill, M. R.; Lashewycz, R. A. *Inorg. Chem.* **1979**, *18*, 3261.

(5) Vits, J. C.; Jacobsen, G.; Dutta, T. K.; Fehlner, T. P. *J. Am. Chem. Soc.* **1985**, *107*, 5563.

(6) VanderVelde, D. G.; Holmgren, J. S.; Shapley, J. R. *Inorg. Chem.* **1987**, *26*, 3077.

0002-7863/94/1516-5414$04.50/0

Scheme 1

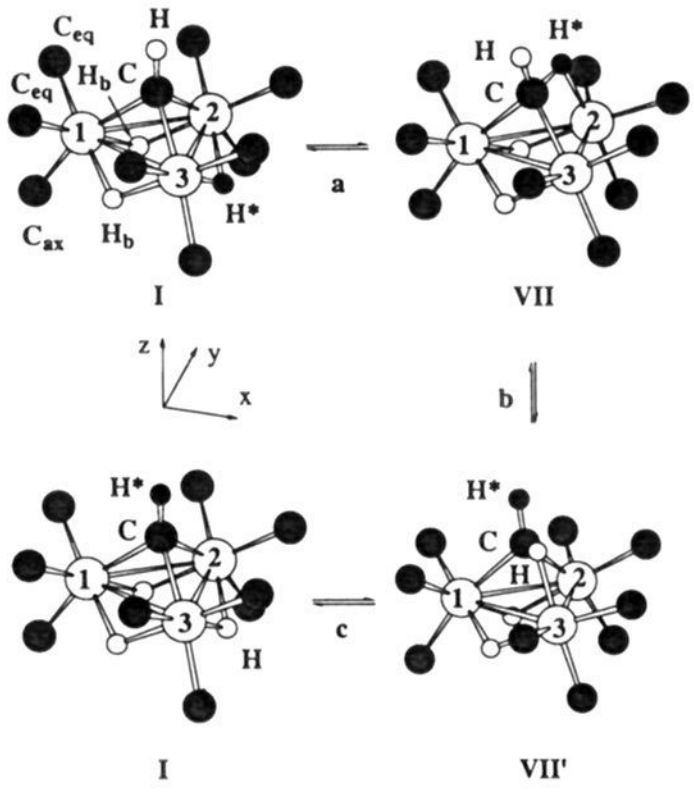

returns to the original structure **2**, denoted **I** from now on, by a reversal of the first step, i.e., a migration (step c) of a hydride from an M–C bond to the nonbridged M–M bond. This mechanism is supported by the fact that it involves some isomers postulated for the Fe corresponding system and ferraboranes.[5] An Fe–C–H interaction has been directly detected for the $Fe_3(CO)_9(\mu_3\text{-}CH_2)(\mu\text{-}H)^-$ anion. Such a mechanism is also reinforced by the fact that the presence of CO does not affect the exchange process, suggesting that the exchange does not take place through a reversible loss of a CO molecule and the formation of a terminal hydride from a bridging one but through a true intramolecular exchange.

The mechanism of Scheme 1 is also consistent with results reported for the similar $Os_3(CO)_{10}(\mu\text{-}H)_2(\mu\text{-}CH_2)$ complex **3**.[7] A neutron diffraction experiment has revealed that the structure in the crystal is well written as **3**.[8] A tautomeric pair can, however, exist in solution: not only the conformation **3** but also an isomer of which the formula can be written as $Os_3(CO)_{10}(\mu\text{-}H)(\mu\text{:}\eta^2\text{-}CH_3)$, obtained by the transfer of a hydride bridging a metal–metal bond into an Os–C bond. This hydride migration, associated with a rotation of the $\mu\text{:}\eta^2\text{-}CH_3$ species, can undergo a hydride exchange in a way similar to the mechanism proposed for 2. Kneuper and Shapley have also investigated the hydride exchange between ring and metal sites in the arene complex $Os_3(CO)_9(\mu\text{-}H)_2(\mu_3\text{:}\eta^2\text{-}C_6H_4)$ and related derivatives[9] and the H/D exchange between ring and metal sites in the benzylidyne complex $Os_3(CO)_9(\mu\text{-}H)_3(\mu_3\text{-}CC_6D_5)$.[10]

We have previously carried out *ab initio* molecular orbital (MO) studies on the electronic structure and the rotational barrier of benzene in the triosmium "helicopter" complex $Os_3(CO)_9(C_6H_6)$, on the geometrical and electronic structures of triruthenium complexes $Ru_3Cp^*_3(\mu\text{-}H)_3(\mu_3\text{-}H)_2$, $Ru_3Cp^*_3(\mu\text{-}H)_6^+$, and $Ru_3Cp^*_3(\mu\text{-}H)_3$, and on the rearrangement of $Ru_3Cp^*_3(\mu\text{-}H)_3(\mu_3\text{:}\eta^2\text{-}HCCR')$.[11] In the present paper, we will focus on and carry out a similar *ab initio* MO study on the H exchange process in the complex $M_3(CO)_9(\mu\text{-}H)_3(\mu_3\text{-}CH)$ (M = Os, Ru). Based on the experimental hypothesis that the exchange takes place through the insertion of a hydride bridging a metal–metal bond into an M–C(H) bond and the rotation of the formed CH_2 species, we considered and determined the possible structures on such pathways in order to obtain a qualitative and quantitative profile of the exchange potential energy surface (PES). After the methods section, we will discuss in detail the geometries and energies of many intermediates and transition states we have obtained for the Os compound. In the following section, we will briefly discuss the Ru analog, which has many similarities to the Os compound.

Methods of Calculations

All the structures have been optimized by an energy gradient method at the RHF level using the Gaussian 90 and Gaussian 92 packages.[12] The metal centers have been described with the relativistic effective core potential of Hay and Wadt, including 60 and 28 core electrons for Os and Ru, respectively, and the associated valence double-ζ quality basis set.[13] The basis sets used for the other atoms are the split-valence 6-31G[14] on the H centers and the methylidyne C center and the minimal STO-3G basis set[15] on the spectator carbonyl ligands. The use of a minimal basis set for spectator ligands not directly involved in a reaction has been justified in several theoretical studies.[11,16] For the reactant complex **I**, we have carried out full geometry optimization under the experimental C_{3v} symmetry. As will be shown later, all the M–C and C–O distances and the M–C–O angles are found to be nearly identical. Therefore, for all subsequent optimizations, we froze them at 1.937 Å, 1.150 Å, and 180.0°, respectively, for Os and 2.002 Å, 1.146 Å, and 180.0° for Ru. These model distances are obtained by averaging the distances obtained in the full optimization calculation for **I**, and the carbonyls are assumed to be linear. In order to include the correlation effects for more reliable energetics, we carried out single-point frozen-core Møller–Plesset second-order perturbation (MP2) calculations at the RHF geometries using the previously described basis set. The identification of some structures optimized under symmetry constraints has been carried out by a partial calculation of the Hessian matrix including only some important degrees of freedom, as will be discussed later.

In the figures presented in this paper, we use bold numbers to show the geometrical parameters of the Os structures and light numbers for Ru ones. Parameters involving the metal centers are written with the Os label. The RHF and MP2 energies, relative to the reactant **I**, of all the calculated structures are summarized in Table 1.

(7) (a) Koike, M. Ph.D. Thesis, University of Illinois, 1991. (b) Calvert, R. B.; Shapley, J. R.; Schultz, A. J.; Williams, J. M.; Suib, S. L.; Stucky, G. D. *J. Am. Chem. Soc.* **1978**, *100*, 6240.
(8) Schultz, A. J.; Williams, J. M.; Calvert, R. B.; Shapley, J. R.; Stucky, G. D. *Inorg. Chem.* **1979**, *18*, 319.
(9) Kneuper, H. J.; Shapley, J. R. *Organometallics* **1987**, *6*, 2455.
(10) Kneuper, H. J.; Shapley, J. R. *New. J. Chem.* **1988**, *12*, 479.
(11) (a) Riehl, J. F.; Koga, N.; Morokuma, K. *Organometallics* **1993**, *12*, 4788. (b) Riehl, J. F.; Koga, N.; Morokuma, K. Submitted for publication.

(12) Frish, M. J.; Head-Gordon, M.; Trucks, G. W.; Foresman, J. B.; Schlegel, H. B.; Raghavachari, K.; Robb, M. A.; Binkley, J. S.; Gonsalez, C.; Defrees, D. J.; Fox, D. J.; Whiteside, R. A.; Seeger, R.; Melius, C. F.; Baker, J.; Martin, L. R.; Kahn, L. R.; Stewart, J. J. P.; Topiol, S.; Pople, J. A. *Gaussian 90*; Gaussian, Inc.: Pittsburgh, PA, 1990. Frish, M. J.; Trucks, G. W.; Head-Gordon, M.; Gill, P. M. W.; Wong, M. W.; Foresman, J. B.; Johnson, B. G.; Schlegel, H. B.; Robb, M. A.; Replogle, E. S.; Gomperts, J. L.; Andres, J. L.; Raghavachari, K.; Binkley, J. S.; Gonsalez, C.; Martin, L. R.; Fox, D. J.; Defrees, D. J.; Baker, J.; Stewart, J. J. P.; Pople, J. A. *Gaussian 92*, Revision A; Gaussian, Inc.: Pittsburgh, PA, 1992.
(13) Hay, P. J.; Wadt, W. R. *J. Chem. Phys.* **1985**, *82*, 299. In order to minimize the atomic energy and reduce the BSSE, some internal s and p functions have been added to the original set given by Hay and Wadt, and the employed basis set can be written as (4111/4111/21) for Os and (3111/3111/31) for Ru. The Os s exponents are 15.414, 9.3776, 3.2241, 1.496, 0.4774, 0.2437, and 0.0583, associated with the contraction coefficients –0.197 70, 0.500 43, –2.046 10, and 2.359 15 for the contracted function; the Os p exponents are 2.194 40, 1.053 20, 0.328 90, 0.146 00, 0.492 30, 0.098 00, and 0.029 00, associated with the contraction coefficients –0.023 49, 0.090 622, –0.588 67, and 1.397 94 for the contracted function; the Ru s exponents are 5.311 50, 2.565, 1.503, 0.5129, and 0.1362, and 0.0417, associated with the contraction coefficients 0.146 10, –2.183 47, and 2.790 01 for the contracted function; the Ru p exponents are 37.705, 4.859, 1.219, 0.4413, 0.1238, and 0.0423, associated with the contraction coefficients –0.007 24, 0.121 40, and 1.065 00 for the contracted function (Riehl, J.-F. Ph.D. Thesis, University of Paris—Orsay, France, 1991).
(14) Hehre, W. J.; Ditchfield, R.; Pople, J. A. *J. Chem. Phys.* **1972**, *56*, 2257.
(15) Hehre, W. J.; Stewart, R. F.; Pople, J. A. *J. Chem. Phys.* **1969**, *51*, 2657.
(16) (a) Koga, N.; Morokuma, K. *Organometallics* **1991**, *10*, 946. (b) Koga, N.; Morokuma, K. *New J. Chem.* **1991**, *15*, 749. (c) Koga, N.; Jin, S.-Q.; Morokuma, K. *J. Am. Chem. Soc.* **1988**, *110*, 3417. (d) Daniel, C.; Koga, N.; Han, J.; Fu, X. Y.; Morokuma, *J. Am. Chem. Soc.* **1988**, *110*, 3773. (e) Koga, N.; Morokuma, K. *J. Am. Chem. Soc.* **1986**, *108*, 6136. (f) Obara, S.; Kitaura, K.; Morokuma, K. *J. Am. Chem. Soc.* **1984**, *106*, 7482. (g) Koga, N.; Obara, S.; Kitaura, K.; Morokuma, K. *J. Am. Chem. Soc.* **1985**, *107*, 7109. (h) Koga, N.; Morokuma, K. *J. Am. Chem. Soc.* **1985**, *107*, 7230.

Table 1. RHF and MP2 Energies Relative to I (in kcal/mol) for the Different Significant Structures Obtained for $M_3(CO)_9(\mu\text{-}H)_3(\mu_3\text{-}CH)$, M = Os, Ru

	$Os_3(CO)_9(\mu\text{-}H)_3(\mu_3\text{-}CH)$		$Ru_3(CO)_9(\mu\text{-}H)_3(\mu_3\text{-}CH)$	
	RHF	MP2	RHF	MP2
I[a]	0.0	0.0	0.0	0.0
II, TS	43.1	25.2	39.8	21.1
III	14.7	14.0	13.3	14.8
IV, TS	47.0	24.9	51.8	19.1
V	12.8	6.7	15.4	6.4
VI, TS	18.1	15.0	19.1	7.9
VII	13.5	14.6	7.9	12.7
VIII, TS	22.8	22.6	19.4	23.0
IX, TS	45.8	21.8	53.0	17.7
X	10.1	6.6	12.9	10.7
XI, TS	47.8	26.3	54.5	10.5
XII	29.1	29.7	26.7	24.6
XIII, top	55.1	36.9	50.7	30.6
XIV, TS	30.1	29.8		

[a] The absolute energies (in Hartrees) of the partially optimized structures I are −1312.856 49 at the RHF level and −1315.218 18 at the MP2 level for the Os compound and −1321.139 77 at the RHF level and −1323.588 64 at the MP2 level for the Ru analog.

Results and Discussion

(I) The $Os_3(CO)_9(\mu\text{-}H)_3(\mu_3\text{-}CH)$ Complex. In order to give a better perspective on the rather complicated mechanism of reaction we have found, in the first subsection we will briefly present the significant intermediate and transition structures in the order they appear on the path from the reactant to the product. The energetics of PES of the entire mechanism will be discussed in the second subsection. The details of the electronic and geometrical structure of each intermediate and transition state will be discussed in the last subsection.

A. Intermediate and Transition Structures. In the rest of this paper, we will adopt the conventions shown in Scheme 1: C will refer to the μ_3-C(H) center and H to the terminal hydrogen connected to C in the reactant, and H* is the chosen bridging hydride to be exchanged with H, usually represented by a black circle in the succeeding drawings. The two remaining bridging hydrides will be referred to as H_b and represented without a label. In some cases, C_{ax} will denote an axial carbonyl ligand and C_{eq} an equatorial carbonyl ligand. The carbonyls or carbonyl carbons at the reaction center are sometimes labeled by X, Y, and Z for easier identification. In the reactant I, $M_3(CO)_9(\mu\text{-}H)_3(\mu_3\text{-}CH)$, assumed to be in C_{3v} symmetry, the C, H, and H* atoms are in one plane perpendicular to the Os_3 plane. As shown in Scheme 1, this plane has been chosen as the xz plane and the metal plane as the xy plane, with the origin N at the center of the metal triangle. Os^2 and Os^3 are the metal atoms bridged by H* in the reactant, and Os^1 is the remaining metal center, which is along the Nx axis in the reactant. A view along the Nz axis of all the relevant RHF optimized structures for the Os analog is depicted in Scheme 2.

As shown in Scheme 2, reactant I can be considered as a six-coordinated octahedral complex; there is no direct formal bonding between metals, and each M is bonded to two μ-H's, one μ_3-CH, and three carbonyl ligands. Starting from reactant I and moving μ-H* in the direction of the metal plane, one reaches the first transition state (TS) II, which has the H* center asymmetrically bonded between Os^2 and Os^3. H* can initially move equivalently either to the right or the left; as shown in Scheme 2, we will assume that H* moves in the direction of Os^2. A symmetric path in which H* moves straight up will be discussed in a subsequent paragraph. In II, H* is almost coplanar with the metal atoms. Following the minimum energy path, or the pseudo-intrinsic reaction coordinate (IRC),[17] from TS II, one finds the first local minimum, intermediate III, in which H* is bonded to Os^2 in a terminal position, roughly in the metal or equatorial plane and *trans* to the bridging hydride H_b. By converting the bridging hydride H* to a terminal hydride, Os^2 now has gained a formal bond with Os^3 and therefore is seven-coordinated. Though II is the transition state for H* dissociation from Os^3 to form seven-coordinated III, if the bond between H* and Os^3 is neglected, the structure of II is similar to the TS for a turnstile rotation connecting two seven-coordinated isomers shown in the next paragraph. Thus II could be regarded as the TS between III and the isomer of the

Scheme 2

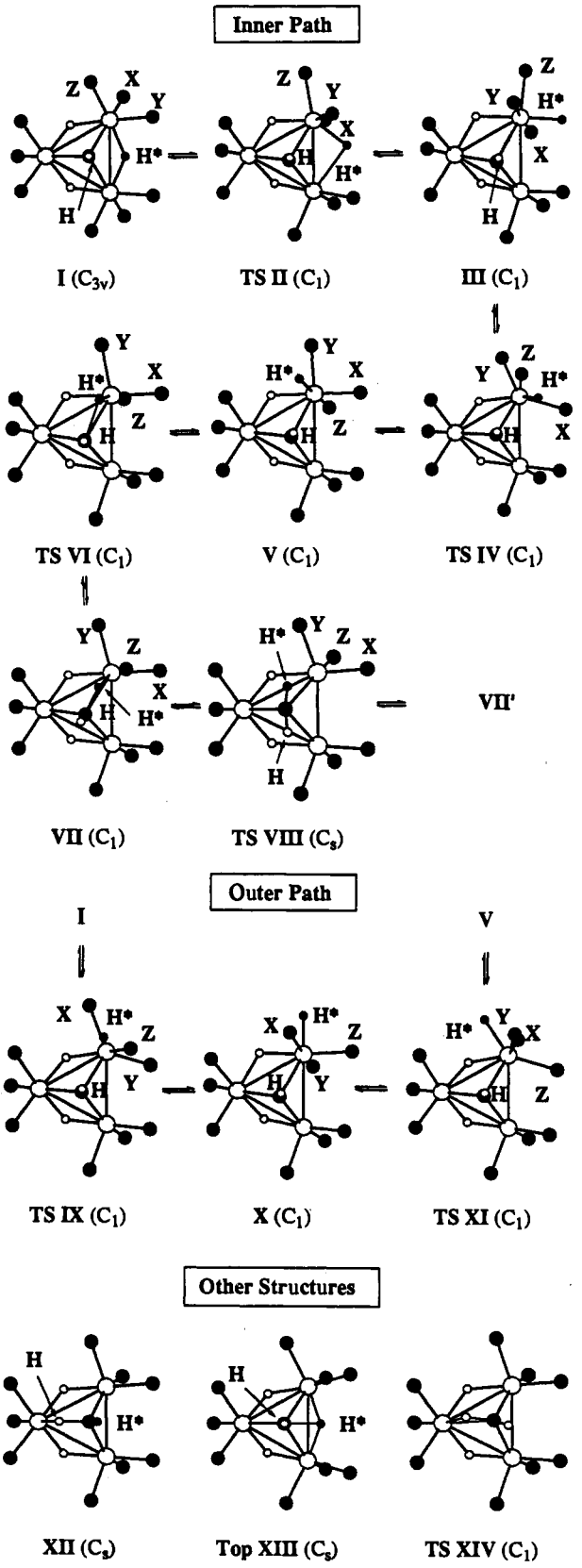

Scheme 3

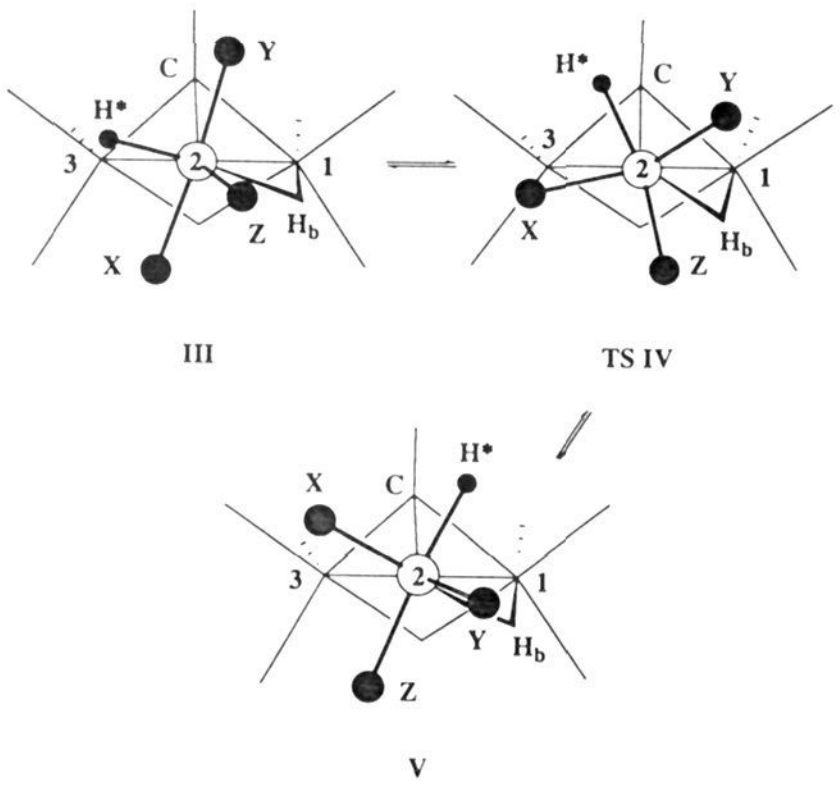

seven-coordinated complex with H* in an axial position below the metal plane, i.e., the position of X in **III** in Scheme 2. But the latter isomer is actually found not to be a local minimum and collapses to **I**, presumably because of the proximity of the two structures. Consequently, **II** is the TS for the combined two steps, H* dissociation from Os^3 (to give this missing isomer) and the turnstile rotation connecting this isomer and **III**.

The second step of the path consists of a turnstile rotation of the $Os^2H^*(CO)_3$ fragment in **III** around the Os^2–P axis, where P is roughly the center of CH_bOs^3 plane, via TS **IV**, to bring H* in the axial position above the metal plane at local minimum **V**. Since the turnstile motion is hard to see in the top view of Scheme 2, it is illustrated in Scheme 3 as a side-view projection along the Os^2–N (the center of the metal triangle) axis, where one can clearly see a clockwise rotation of the four ligands H*, Y, Z, and X. From **V**, it is then possible to insert H* into the Os^2–C bond through TS **VI** to obtain stable intermediate **VII** with an Os–H*–C bridge. As shown in Scheme 1, this structure is nothing but the intermediate postulated in the experimental studies. It should be noted that, going from reactant **I** to intermediate **VII**, one has accomplished not only the transfer of H* from the Os^2–Os^3 bond to the Os^2–C bond but also an exchange of the three carbonyl ligands by a 120° rotation clockwise when seen along the Os^2–N axis; for instance, the originally axial carbonyl X now sits at an equatorial position *cis* to Os^3.

The final exchange itself takes place from **VII**, via a rotation of the CHH* unit, through TS **VIII** of C_s symmetry to the enantiomeric structure **VII′**, in which H is now inserted into the Os^3–C bond and the C–H* bond is terminal. From **VII′**, one can return to reactant **I**, with H and H* exchanged and reacting this time on the Os^3 side, by a reversal of the sequence just described. This mechanism will be called the "inner" mechanism, because the reacting H* travels through the "inside" or the Os^2–Os^3 side.

The stability of seven-coordinated species gives rise to another mechanism. As seen in Scheme 2, the seven-coordinated complex **III** has H* roughly in the equatorial plane and *cis* to Os^2–Os^3. Isomer **X** with H* roughly in the equatorial plane and *trans* to Os^2–Os^3 is also found to be a stable intermediate. As shown in Scheme 2, the reaction mechanism involving this intermediate starts at reactant **I**, moves the bridging H* down away from the metal plane and toward Os^2, and finally reaches the transition state **IX**. TS **IX** is seven-coordinated and is a transition state for the trunstile rotation of the $H^*(CO)_3$ fragment around the Os^2–P axis, as **IV** was. At **IX**, H* moves from the axial position below the metal surface to the equatorial position, i.e., counterclockwise when seen along the Os^2–N axis. The missing isomer, mentioned above, of the seven-coordinated complex with H* in an axial position below the metal plane looks like a feasible precursor of **IX**. Though it does not exist, this mechanism from **I** goes through this region of geometry before arriving at TS **IX**. One can say that in the first half of this step the H* dissociates from Os^3 and in the second half the turnstile rotation takes place. Completing the turnstile motion, the system reaches intermediate **X**. The turnstile rotation of the $H^*(CO)_3$ fragment continues from **X** further in the same direction to reach TS **XI** and finally intermediate **V**. At **V**, this mechanism merges with the inner mechanism and follows the path **V** → **VI** → **VII** → **VIII** → **VII′**, discussed above. In the present mechanism, which will be called the "outer" mechanism, H* travels through the "outside", or away from the Os^2–Os^3 side. While the inner path **I** → **II** → **III** → **IV** → **V** rotates the carbonyl ligands clockwise by 120°, the outer path **I** → **IX** → **X** → **XI** → **V** rotates the carbonyls counterclockwise by 240°. The transition structures of two paths show some geometrical differences because of the difference in the distance traveled by H* from one intermediate to another. For instance, going from **I** to **IX**, H* has to travel a long distance from the bridging position to the outer equatorial position, whereas from **I** to **II**, H* moves a short distance from the bridging to the inner equatorial position. Therefore, TS **IX** is further away from **I** in structural parameters than TS **II**. Despite of differences in the distance H* travels, all the TSs have been confirmed, by following the pseudo-IRC,[17] to reach the designated reactant and product intermediates. In either mechanism, the stereochemical arrangement of H* and three carbonyl groups is the same, in the order of H*YZX clockwise when seen along the Os^2–N axis, as shown for intermediate **V** in Scheme 3.

An extensive RHF search failed to yield a TS which leads directly and in a single step from **I** through a nonsymmetric (C_1) pathway to **VII** by moving H* not too far from the *xz* symmetry plane. This means that any such assumed "path" is higher in energy than the multistep paths just discussed, and optimization of all geometrical parameters from such a "path" puts the system back into the multistep "inner" path. Though there is a slight possibility that a search with a correlated method such as MP2 could have found such a TS, it is rather unlikely that any low-energy TS for such a process exists. Thus this H* insertion must be intrinsically a multistep process.

In addition, we also investigated the pathway, maintaining the C_s symmetry, to move H* upward from reactant **I**, form an HCH* complex, tilt HCH* within the C_s mirror plane, and insert H into the Os^1–C bond to form a complex **XII**. This path could be regarded as the extreme of the nonsymmetric single-step path just discussed above. We could locate such a "C_s transition state" **XIII**, but **XIII** is high in energy,[37] kcal/mol at the more reliable MP2 level above **I**, and actually is not a real TS but a second-order top having an extra a″ imaginary frequency in addition to an a′ imaginary frequency corresponding to the above-mentioned motion of H*. The motion from **VIII** along the a′ mode to both directions leads downhill to **I** and **XII** on each end. As soon as the symmetry is allowed to be broken, **VIII** converges to the previously found complex **VII**, and the reaction path becomes the multistep inner pathway determined above. The intermediate **XII** with a hydride bridging Os^1–C was found to be connected to the intermediate **VII** with a hydride bridging Os^2–C through a transition state **XIV**. Therefore, **XII** should be considered to be a side intermediate of the hydride exchange reaction.

(17) We need here to comment on the expression "following the pseudo-IRC". Due to the size of the system, we could not carry out the calculation using a real IRC algorithm like the one proposed by Ishida et al. or Gonsalez et al. (ref 18). In a simpler way, we distorted the structure of the transition state along the reaction coordinate, the normal coordinate of imaginary frequency of the estimated Hessian, and carried out from there a geometry optimization looking for a minimum.

(18) (a) Ishida, K.; Morokuma, K.; Komornicki, A. *J. Chem. Phys.* **1977**, *66*, 2153. (b) Gonzalez, C.; Schlegel, H. B. *J. Chem. Phys.* **1989**, *90*, 2154.

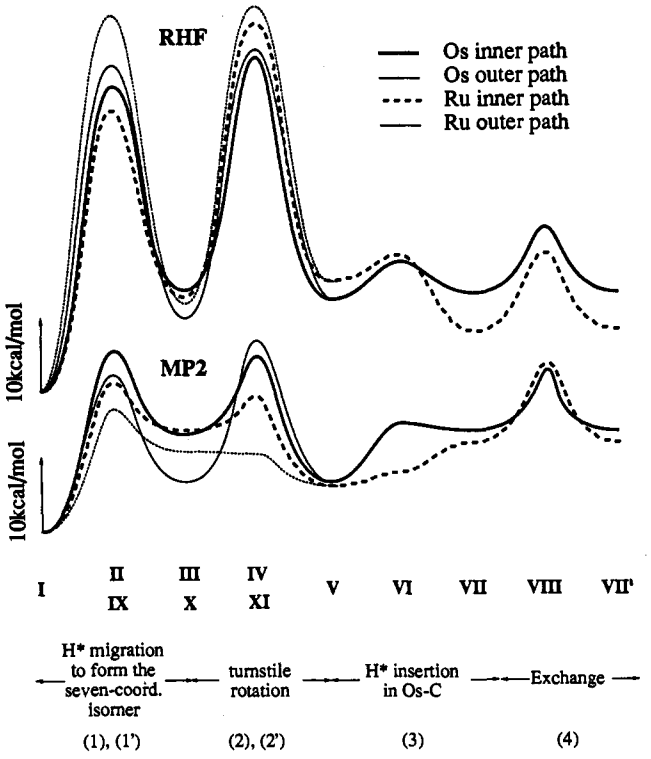

Figure 1. Potential energy profiles along the exchange pathways. Solid lines are for Os and dashed lines for Ru. The upper part shows the RHF energies and the lower part the more reliable MP2 energies. In the first half, related to the seven-coordinated isomers, bold lines are for the inner path and light lines for the outer path.

Structural parameters of **XII**, **XIII**, and **XIV** are given in the supplementary material.

B. Exchange Potential Energy Surface. In this subsection, we discuss the energetics of the H exchange pathways. Energies calculated at the MP2 level including electron correlation as well as at the RHF level at the RHF optimized geometries are summarized in Table 1 and shown in Figure 1. We will base our discussion on the more reliable MP2 energetics.

Our previous discussions and Figure 1 indicate that the hydride exchange reaction takes place in two pathways, each with four steps involving three intermediates and three transition states to reach the midpoint transition state of the reaction, **VIII**, and the second half of this degenerate exchange reaction is the reverse of the first half after exchanging H* and H. The first step is the decoordination of the bridging H center from one metal of reactant **I** to form an M–H terminal bond and a seven-coordinated species. As shown in Table 1, this step has to go over a barrier, **II** of 25 kcal/mol for the inner path and **IX** of 22 kcal/mol for the outer path. Considering that the first step of both paths involves some turnstile rotation as well as the hydride migration, the barrier is surprisingly low in energy. This first step for both pathways has the largest activation energy on the exchange PES and therefore should be the rate-determining step. For the present Os complex, the inner and outer pathways have similar energetics, and the preference of the one over the other does not seem to be large. The intermediates **III** and **X** thus formed have a substantial kinetic stability and may be observable experimentally. The second step, the turnstile rotation of the $H^*(CO)_3$ fragment around the Os^2–P axis, goes over TS **IV** and **XI** and requires the activation energy of 11 and 20 kcal/mol for the inner and the outer paths, respectively. The resultant intermediate of the both pathways, **V**, seems to have a substantial kinetic stability and may also be observable.

The third step of the reaction is the insertion of H* into the Os^2–C bond and has a low barrier at **VI**. The product of this insertion reaction is the intermediate **VII** suggested by the experimentalists. The barrier for the reverse process is very low, 0.4 kcal/mol, suggesting that this species is probably not kinetically stable or that the minimum may disappear at a better level of calculation and become an "inflection point" on the PES. The fourth and final step of the first half of the degenerate exchange reaction is the exchange of the two hydrides in the HCH* group via the C_s-symmetric TS **VIII**. The activation barrier to this step is 8 kcal/mol, much lower than that to the first step.

The calculated barrier for the entire reaction, 22–25 kcal/mol, is in very good agreement with the experimental enthalpy of activation of 24.0 ± 1.7 kcal/mol. This agreement suggests that, though we have not explored all the other possible mechanisms of this exchange reaction, which would be impossible for these kinds of complicated systems, the mechanism proposed here is likely to be quite realistic.

C. Detailed Discussions of Intermediates and Transition States. In this section, we will discuss in detail the structural and energetical features of various intermediates and transition states.

Reactant I. X-ray and neutron diffraction experiments have established that the most stable structure of $Os_3(CO)_9(\mu\text{-}H)_3(\mu_3\text{-}CH)$ has C_{3v} symmetry.[19] As already discussed, all the carbonyl ligands are terminal and nearly linear, six being *cis* to the Os–C bonds and referred to as equatorial carbonyls C_{eq}, and three being axial carbonyls C_{ax} *trans* to the Os–C bonds. The three Os–Os bonds are bridged with hydrogen atoms. Geometrical parameters optimized at the RHF level shown in Figure 2 are qualitatively in good agreement with the experimental data and follow the general trend we already found and discussed in previous calculations of trimetallic clusters;[11] though the angular parameters are quite accurately reproduced, the bond lengths are found to be too long: +0.064 Å for the Os–Os distance (2.957 Å calculated vs 2.893 Å experimental), +0.029 Å for the Os–C distance (2.130 Å calculated vs 2.101 Å experimental), and +0.046 Å for the average Os–C(O) distance. The Os–(μ-H) distance is, however, properly reproduced: 1.840 Å calculated vs 1.834 Å experimental obtained by a neutron diffraction experiment. This distance is consistent with M–H distances observed in other compounds, e.g., 1.845(3) Å in $Os_3(CO)_{10}(\mu\text{-}H)_2$.[4a] These distances are longer than the terminal Os–H distance, for which Orpen et al. reported a value of 1.659 Å as an average of four observations.[20]

Bond and dihedral angles given in Figure 2 and Table 2 show that the Os centers are in a fairly regular octahedral ligand field, which is consistent with their formal oxidation state of 2+. Though we systematically represented the M–M bonds in this and subsequent figures for easier understanding of the geometry, the Os–Os bonds are formally broken when they are bridged by a hydride, despite the apparent short metal–metal distance; the Os–Os separation in **I** is in fact of the order of a typical σ single Os–Os bond like in $Os_3(CO)_{12}$, 2.945 Å calculated[1] and 2.877 Å experimental.[1a] Such a distance in **I** is actually the result of cycle constraint due to the H and CH bridging ligands. The effect of such a constraint or multicentered bond can be substantial. For instance, in the binuclear $Ru_2Cp^*_2(\mu\text{-}H)_4$ complex with a Ru–Ru separation of 2.43 Å,[21] Koga and Morokuma showed that there is formally no d–d direct Ru–Ru bond.[22] Such a behavior has also been observed in cyclopentadienyltriruthenium clusters: the Ru–Ru separation is shorter in the hexahydride $Ru_3Cp_3(\mu\text{-}H)_6^+$ than in the trihydride $Ru_3Cp_3(\mu\text{-}H)_3$ because of the larger constraints.[11] In **I**, the geometry of the $Os_3(CO)_9$ unit is quite different from that of the free fragment. The calculated C_{ax}–Os–N angle, where N is the center of the Os_3 triangle, is 122.5° in **I**, but 97.8° in $Os_3(CO)_9$ using the same level of calculation.[11]

(19) Orpen, A. G.; Koetzle, T. F. *Acta Crystallogr.* **1984**, *B40*, 606.
(20) Orpen, A. G.; Brummer, L.; Allen, F. A.; Kennard, O.; Watson, D. G.; Taylor, R. *J. Chem. Soc., Dalton Trans.* **1989**, Suppl. S1.
(21) Suzuki, H.; Omori, H.; Lee, D. H.; Yoshida, Y.; Moro-oka, Y. *Organometallics* **1988**, *7*, 2243.
(22) Koga, N.; Morokuma, K. *J. Mol. Struct. (Theochem)* **1993**, *300*, 181.

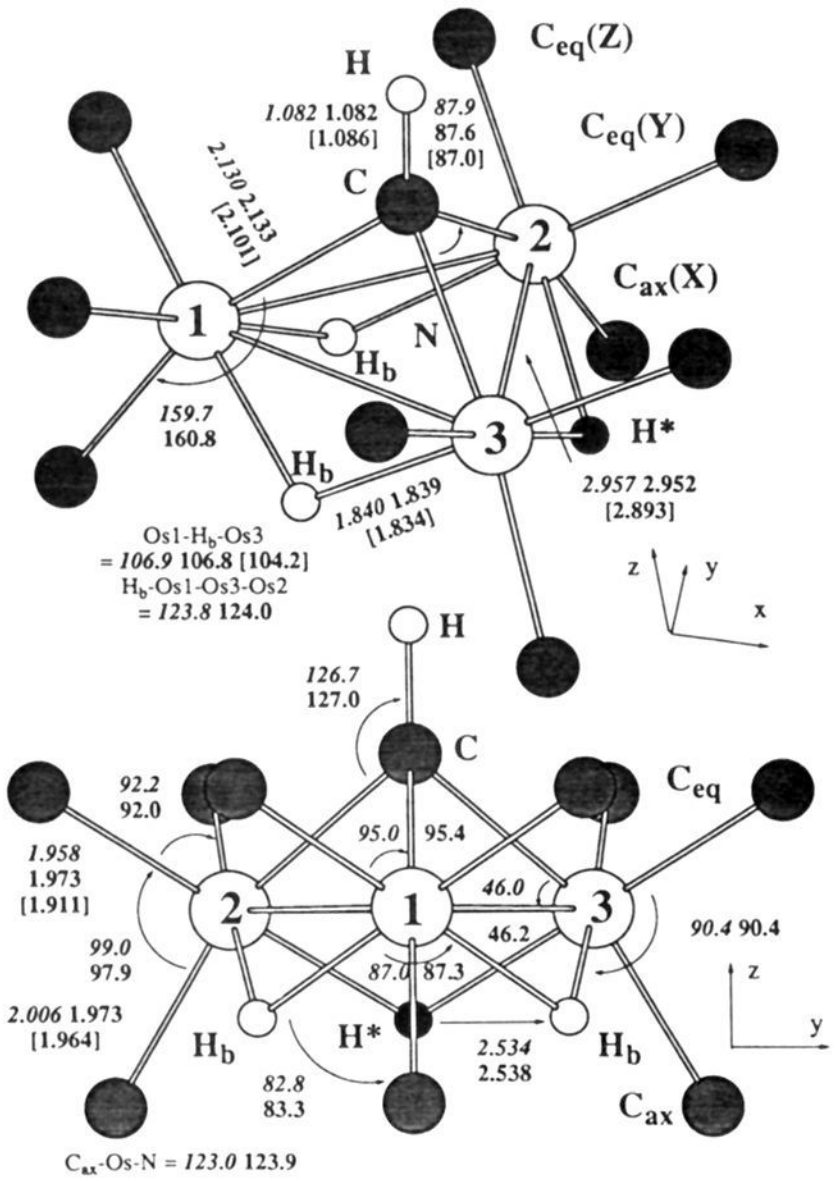

Reactant I (C_{3v} assumed)

Figure 2. Two views of the RHF optimized C_{3v} structure of the reactant $Os_3(CO)_9(\mu\text{-}H)_3(\mu_3\text{-}CH)$ (**I**). In italics are the preliminary fully optimized geometry values. Experimental parameters are in square brackets. Distances are given in angstroms and angles in degrees. N is the center of the metal triangle.

Intermediates III, V, and X with Seven-Coordinated Os Atom. Structures **III**, **V**, and **X**, sketched in Scheme 2 and given in Figures 3 and 4 and the supplementary material, respectively, are all stable intermediates, seven-coordinated at Os^2 with H* in a terminal position, and can be written as $Os_3(CO)_9(\mu\text{-}H)_2H(\mu_3\text{-}CH)$. The generation of seven-coordinated structures can formally be accomplished by the addition of a ligand to a regular octahedron.[23] The addition on an octahedral edge leads to a D_{5h} pentagonal bipyramid (PBP), while the face attack leads to a capped octahedron or a capped trigonal prism (CTP).

For **III**, one can see in Figure 3 and Table 2 that the three carbonyls and the two hydrides connected to Os^2 are in a square-pyramid (SP) disposition, the Os^2–Z being the pyramid axis. Carbonyls X and Y are in a *trans* arrangement and are both axial ligands, Os–X and Os–Y bonds being roughly perpendicular to the metal plane. The two other ligands connected to Os^2, C and Os^3, are capping this SP. If C and Os^3 are considered to form a parallel line with the above-mentioned square, the ligand field around the seven-coordinated Os^2 is nothing but a distorted CTP, with Z as the capping ligand. In a different perspective, if one considers the plane formed by Y–Z–X–Os^3–C as the pentagon and H* and H_b as the apical ligands, as suggested by the H*–Os^2–H_b angle of 173.7°, the ligand field around Os^2 can be also viewed as a distorted PBP.

We now discuss and compare the electronic structures of **III** and **I**. In **I**, the metal centers are in an octahedral ligand field and are formally Os^{2+} (d^6). As represented in **4**, 12 electrons in three Os–C bonds and three 3-center 2-electron Os–H–Os bonds are responsible for the binding of the $Os_3(\mu\text{-}H)_3(\mu_3\text{-}CH)$ unit. In **III**, on the other hand, there is a covalent bond between Os^2 and Os^3, and, as represented in **5**, 14 electrons in three Os–C bonds, two 3-center 2-electron Os–H–Os bonds, one Os–Os bond, and one Os–H bond are responsible for the binding of the $Os_3(\mu\text{-}H)_2H(\mu_3\text{-}CH)$ unit. This implies that the oxidation state of Os^2 is formally 4+ (d^4), while Os^1 and Os^3 remain d^6.

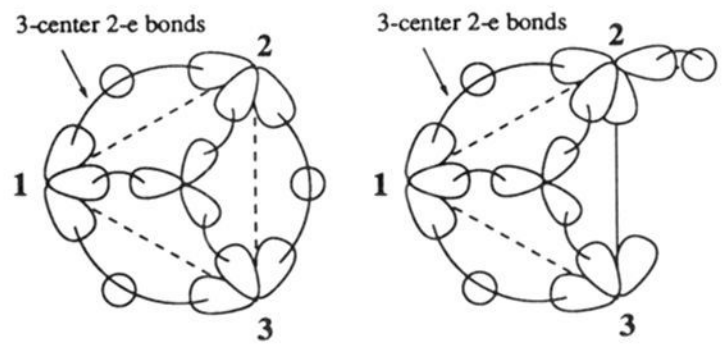

4 **5**

While **III** has the terminal H* in an equatorial position in the inner region or the region close to Os^2–Os^3, **X** has the terminal H* in an equatorial position in the outer region or the region away from Os^2–Os^3, and **V** has the terminal H* occupying an axial position above the metal plane. Nevertheless, **V** and **X** are very similar in structure to **III**. On the other hand, **III** is less stable than **V** and **X**, because in **III** the terminal H* with strong *trans* influence and the bridging H_b are *trans* to each other.

One can also consider the local geometries of **III**, **V**, and **X** at Os^2 as various isomers of an octahedral complex have three carbonyls, two hydrides, and Os^3 ligands, with a secondary interaction with Os^1 and C. Of four possible isomers having Os^3 and H in *cis* disposition, three are nothing but **III**, **V**, and **X**; the one missing with three carbonyls in *mer* diposition and H* below the metal plane corresponds to the structure between the reactant **I** and TS **IX** for the outer path and will be discussed again in connection to the TS **IX**.

Transition States IV and XI for Turnstile Rotation. Following the inner path farther from seven-coordinated **III**, our RHF TS optimization found transition state **IV**, which was confirmed to connect **III** and another seven-coordinated intermediate, **V**. The geometry of this TS **IV** is shown in Figure 5. For the outer path, we also found TS **XI**, sketched in Scheme 2 and given in the supplementary material, between **X** and **V**. Though there are some small structural differences between TS **XI** and TS **IV**, both of them are TSs for turnstile motion around the seven-coordinate Os^2, moving H* from the equatorial to the axial position above the metal plane, on the nonbridged Os^2–Os^3 side for **IV** and on the H-bridged Os^2–Os^1 side for **XI**.

We will now continue on TS **IV**. Ligand exchange in a seven-coordinated species is still an open question and was recently studied with the prototype of the seven-coordinated species, IF_7.[24] This molecule is known to adopt the pentagonal-bipyramidal geometry. Christe et al.[24] proposed a mechanism for the axial–equatorial ligand exchange as a combination of an axial and equatorial bending, analogous to the Berry mechanism for the axial–equatorial exchange in the trigonal bipyramid.[25] The present $Os_3(CO)_9(\mu\text{-}H)_2H(\mu_3\text{-}CH)$ is expected to pose more complications because three of the seven ligands around Os^2, i.e., C, H_b, and Os^3, are connected to the rest of the cluster both in reactant **III** and in product **V** of the present step and cannot be easily deformed without causing strain in the cluster. The remaining four ligands, H* and the three carbonyls, are terminal and can, in principle, be moved without strain. Actually, TS **IV** between **III** and **V** is in the process of moving these four "mobile"

(23) Hoffmann, R.; Beier, B. F.; Muetterties, E. L.; Rossi, A. R. *Inorg. Chem.* **1977**, *16*, 511.

(24) Christe, K. O.; Curtis, E. C.; Dixon, D. A. *J. Am. Chem. Soc.* **1993**, *115*, 1520.

(25) Berry, R. S. *J. Chem. Phys.* **1960**, *32*, 933.

Table 2. L–Os²–L′ Angles and L–Os²–C–H Dihedral Angles (in degrees) for the Intermediate and Transition Structures Involved in the Exchange Path

	inner path							outer path				
	I	**TS II**	**III**	**TS IV**	**V**	**TS VI**	**VII**	**I**	**TS IX**	**X**	**TS XI**	**V**
					L–Os²–L′ Angles							
CO(X), CO(Y)	97.9	142.3	175.1	130.4	96.9	96.2	97.1	97.9	126.5	166.6	132.4	96.9
CO(X), CO(Z)	97.9	91.1	89.4	80.4	97.9	94.5	92.6	97.9	87.8	92.2	90.2	97.9
CO(X), H*	93.3	76.2	88.5	75.7	85.1	87.0	88.1	93.3	78.8	84.3	76.0	85.1
CO(X), H bridging	83.3	80.6	85.2	134.8	178.2	176.9	175.3	83.3	84.5	91.3	133.0	178.2
CO(X), C(H)	160.8	130.6	110.7	108.9	97.1	103.8	103.1	160.8	114.9	75.2	76.9	97.1
CO(Y), CO(Z)	92.0	86.3	90.4	93.0	94.8	101.0	101.4	92.0	90.1	92.9	84.5	94.8
CO(Y), H*	90.4	79.7	86.7	76.5	80.6	88.3	91.7	90.4	73.9	83.2	78.3	80.6
CO(Y), H bridging	177.2	135.8	99.7	89.8	84.2	83.4	84.5	177.2	119.5	82.2	74.3	84.2
CO(Y), C(H)	95.4	75.5	70.7	98.5	145.3	124.8	114.2	95.4	116.0	114.7	150.1	145.3
CO(Z), H*	177.2	139.9	90.4	141.2	174.8	170.4	166.7	177.2	146.2	91.9	140.0	174.8
CO(Z), H bridging	90.4	81.8	89.5	72.6	83.4	82.5	82.7	90.4	147.5	172.2	135.1	83.4
CO(Z), C(H)	95.4	130.0	155.5	149.4	114.4	127.3	138.4	95.4	75.0	107.6	104.3	114.4
H*, H bridging	87.3	135.1	173.7	142.9	93.8	96.1	96.3	87.3	62.3	81.6	73.8	93.8
H*, C(H)	82.9	86.5	103.4	69.3	69.2	43.3	29.4	82.9	138.8	151.9	108.5	69.2
H, C(H)	82.9	80.2	78.9	79.2	81.2	78.9	80.1	82.9	79.8	80.0	79.6	81.2
					Dihedral Angles[a]							
CO(X)	180.0	166.2	159.0	94.3	57.3	56.8	52.6	180.0	−54.8	−27.4	2.5	57.3
CO(Y)	46.2	17.5	−15.9	−43.6	−59.6	−51.0	−51.5	46.2	108.2	162.0	−166.5	−59.6
CO(Z)	−46.2	−54.9	−57.3	−154.6	155.7	163.6	162.0	−46.2	25.5	60.2	89.3	155.7
H*	135.9	97.7	65.6	28.4	−28.3	−13.4	−8.5	135.9	−156.7	−71.8	−67.6	−28.3

[a] H–C–Os²–L dihedral angles. Positive angles are for ligands on the side of the HCOs² plane containing Os³; negative angles are for ligands on the side of the HCOs² plane containing H_b.

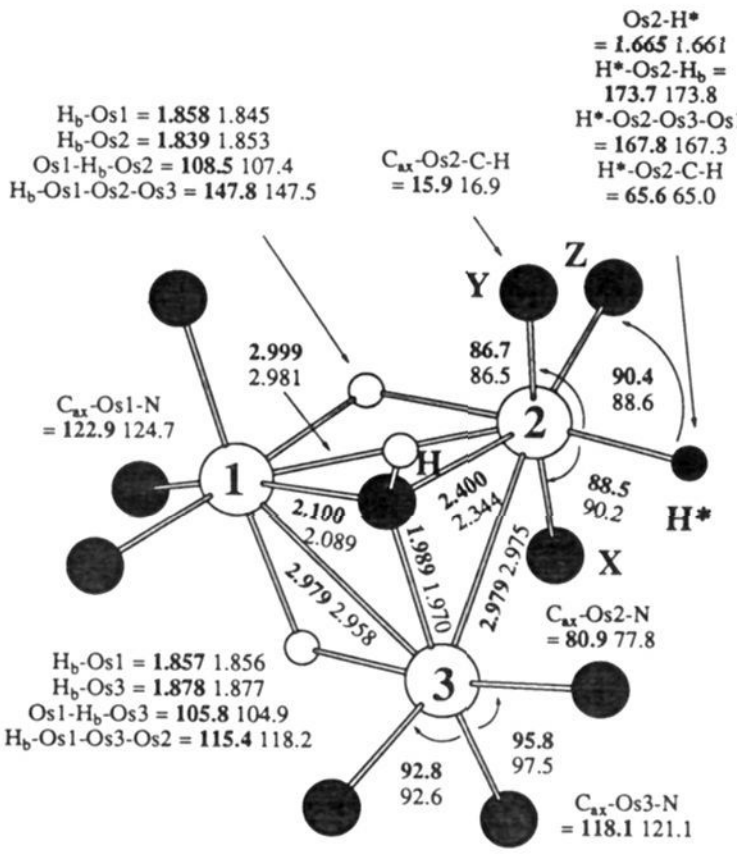

III (C_1)

Figure 3. RHF optimized structure of the seven-coordinated intermediate **III** for Os (bold) and Ru (light). Distances are given in angstroms and angles in degrees. N is the center of the metal triangle.

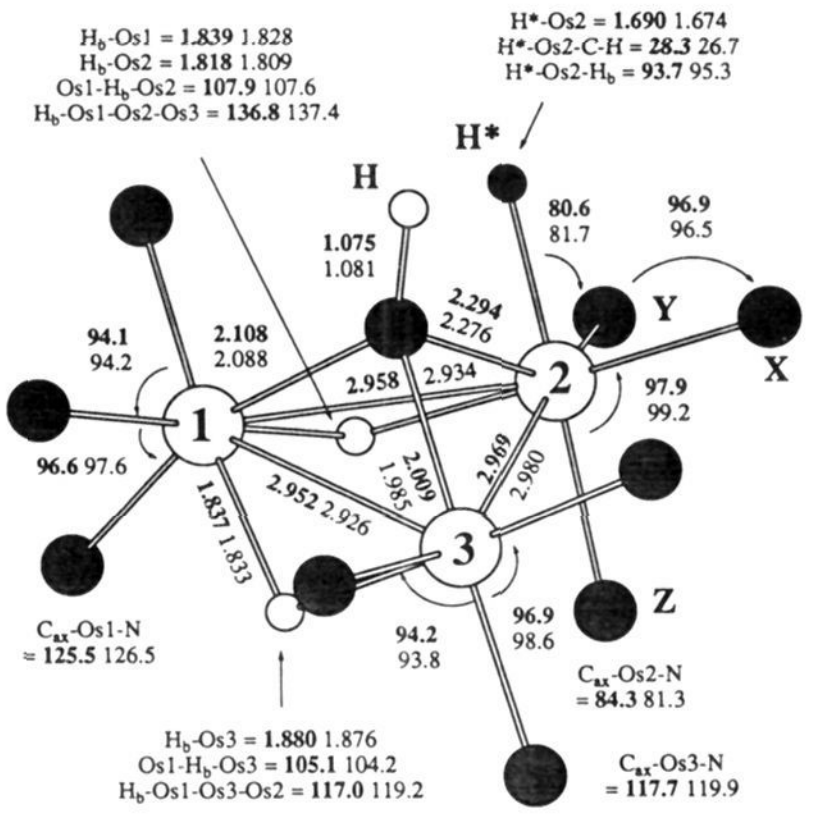

V (C_1)

Figure 4. RHF optimized structure of the seven-coordinated intermediate **V** for Os (bold) and Ru (light). Distances are given in angstroms and angles in degrees. N is the center of the metal triangle.

ligands in a turnstile fashion of rotation, as seen qualitatively in the side view in Scheme 3 and the top view in Scheme 2 as well as more quantitatively in bond and dihedral angles in Table 2. At first, the angle between the equatorial ligands, i.e., ∠(Z–Os²–H*), opens from 90.4° in **III** to 141.2° in **IV**, and the angles between the axial ligands, i.e., ∠(X–Os²–Y), closes from 175.1° in **III** to 130.4° in **IV**, to place these four ligands at the corners of a square in a pseudo-C_{4v} symmetry, and this square rotates around an Os²–P axis by about 45°. The logical choice for P would be the center of the plane defined by the three "immobile" ligands, which should not be very different from the center of the Os_3 plane, designated as N before. The side view of Scheme 3 is along the Os²–N axis and suggests that the above interference is essentially correct. The opening and closing of the bond angles and the turnstile rotation need not take place sequentially, and probably they actually occur concurrently. Form TS **IV** to intermediate **V**, one makes an additional 45° turnstile rotation in the same direction, closes the X–Os²–Y angle further to 96.9°, and opens the Z–Os²–H* angle further to 170.4°.

During this step, the geometry of the nonreactive $Os_2(CO)_6(\mu\text{-}H)_2(\mu_3\text{-}CH)$ fragment of the structure changes little. There are some noticeable changes in the geometrical parameters connecting this fragment with the reacting $Os^2(CO)_3H^*$ fragment. For instance, the Os²–Os³ distance decreases from 2.979 Å in **III** to 2.862 Å in TS **IV** and increases again to 2.969 Å in **V**. A shorter Os²–Os³ distance at the TSs than at the intermediates is a common feature found for all the turnstile isomerization steps discussed in this paper, including **X** → **XI** → **V** as well as **I** →

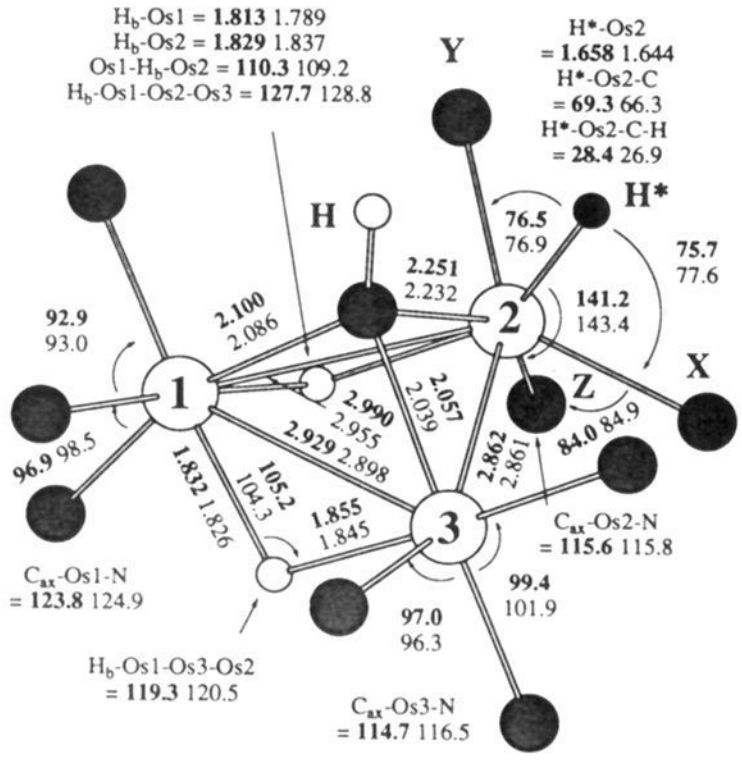

TS IV (C_1)

Figure 5. RHF optimized structure of the transition state **IV** between **III** and **V** for turnstile rotation in the inner path for Os (bold) and Ru (light). Distances are given in angstroms and angles in degrees. N is the center of the metal triangle.

II → **III** and **I** → **IX** → **X**. The last two steps will be discussed in the following section.

The presently proposed mechanism of isomerization of a seven-coordinated complex can be compared with the Berry pseudorotation mechanism of isomerization of five-coordinated TBP mononuclear transition-metal complexes.[16c] There, at first the L_{ax}–M–L_{ax} bond angle closes from around 180°, and one of the L_{eq}–M–L_{eq} bond angles opens up from around 120° to reach the transition state having an SP structure with the third L_{eq} taking up the axial pivot position, and then, continuing the motion, the L_{ax}–M–L_{ax} bond angle reaches around 120°, putting the pair of former axial ligands in the equatorial positions, and the L_{eq}–M–L_{eq} bond angle becomes around 180°, placing the former equatorial ligand pair in the axial positions. This process is usually associated with a very low intrinsic barrier. In the present isomerization, as discussed above, essentially the same bond angular changes take place from the reactant to reach an SP structure consisting of the Os^2 metal center and the four "mobile" ligands. In the present case, however, the equatorial ligands cannot continue opening up their bond angle, because the existence of three "immobile" ligands in the vicinity of the equatorial plane prevents such an excessive opening. Therefore, the square made of the four "mobile" ligands at first has to make a 90° turnstile rotation to move the former equatorial ligands to axial positions before continuing the bond angular change. This requirement of the additional turnstile rotation must be the origin of a higher barrier here than in the TBP mononuclear complex.

Transition States II and IX from Reactant I. Starting from reactant **I**, TS **II**, belonging to the inner path, is the first transition state one reaches when H* is moved up toward the metal plane in the direction of Os^2–Os^3. As shown in Figure 6, the migrating H* has already moved up close to the Os_3 plane, as indicated by the H*–Os^2–Os^3–Os^1 dihedral angle of 176.3°. H* is asymmetrically bonded to Os^2 and Os^3, with the Os^2–H* and Os^3–H* distances of 1.689 and 2.311 Å, respectively. These values suggest that the Os^3–H* bond is almost broken and that the Os^2–H* bond is nearly terminal, only slightly longer than a typical Os–H terminal bond distance of 1.659 Å.[20] This also implies that the Os^2–Os^3 bond has already been formed. Actually, the Os^2–Os^3 distance in **II** is 2.890 Å, shorter than that in **I** by 0.07 Å. Qualitatively speaking, the Os^2 fragment in **II** is already close to a seven-coordinated species.

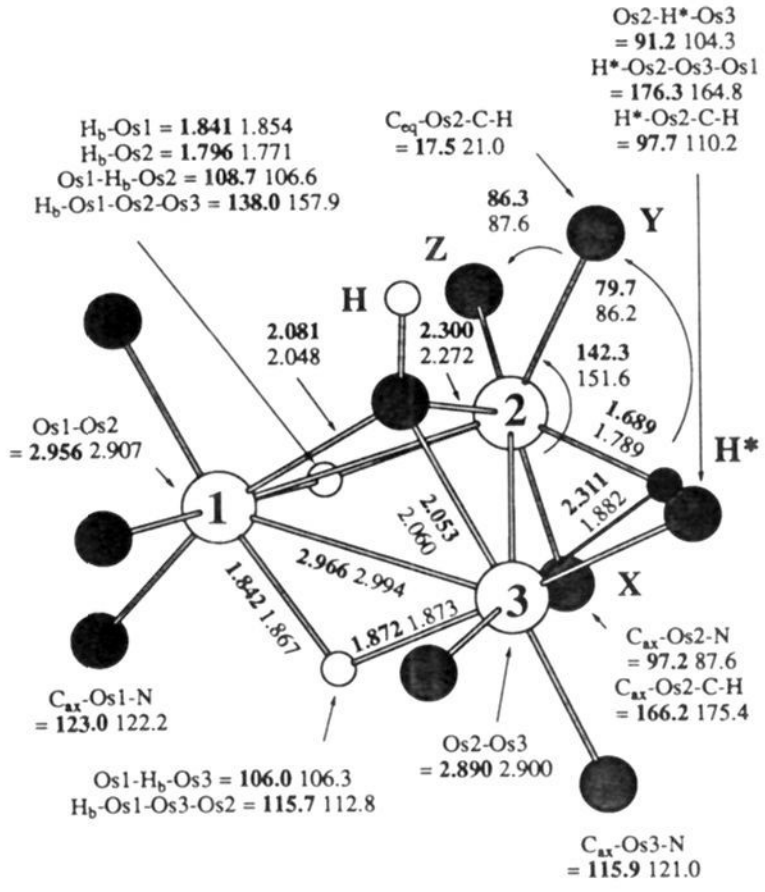

TS II (C_1)

Figure 6. RHF optimized structure of the transition state **II** between **I** and **III** for H* migration in the inner path for Os (bold) and Ru (light). Distances are given in angstroms and angles in degrees. N is the center of the metal triangle.

One can see in Figure 6 and Table 2 a substantial distortion of the $Os^2(CO)_3$ unit, which is adjusting Os^2 for the final seven-coordinated ligand field. As shown in Scheme 2, the carbonyl X in **I** has moved little in **II**; the C_{ax}–Os^2–C–H dihedral angle is 166.2° in **II** vs 180° in **I**. The equatorial carbonyl Y *cis* to H* in **I** has, however, moved toward C–H and is close to an axial position, as shown by the 142.3° C_{ax}–Os^2–C_{eq} angle and the 17.5° C_{eq}–Os^2–C–H dihedral angle. Coordination of H* in a terminal position also weakens the Os^2–C bond, as suggested by 2.300 Å in **II** vs 2.133 Å in **I**.

These structural features suggest that **II** is similar to the TSs for turnstile rotation, **IV** and **XI**; the 142.3° X–Os^2–Y angle and the 139.9° Z–Os^2–H* angle indicate that the ligands, X, Y, Z, and H*, constitute the square which rotates during the turnstile motion. One end of the turnstile rotation is intermediate **III**, and the other is the fourth possible but missing isomer of the seven-coordinated species with H* in an axial position under the metal plane. If this existed, the reaction from **I** to **III** could consist of two separate steps, H* migration to Os^2 between **I** and the fourth isomer and then turnstile rotation to reach **III**. The fourth isomer is not a stable intermediate, and therefore these two steps are combined.

Structure **IX**, sketched in Scheme 2 and given in the supplementary material, belongs to the outer path starting from reactant **I**. **IX** is the TS for the combined two steps, the H* migration between **I** and the fourth, missing seven-coordinated isomer, exactly the same step to that in the inner path just discussed, and the turnstile rotation, in the direction opposite to that in the inner path, to reach **X**. Because of the larger amplitude of turnstile rotation, **IX** is located more in the region of turnstile rotation.

Transition State VI and Intermediate VII. As already depicted in Scheme 2, from intermediate **V**, which has H* in the axial position above the metal plane, one can finally proceed to insert H* into the Os^2–C bond through the transition state **VI** given in Figure 7 to reach the third stable intermediate **VII** in Figure 8. TS structure **VI** shows that H* is moving toward C and also

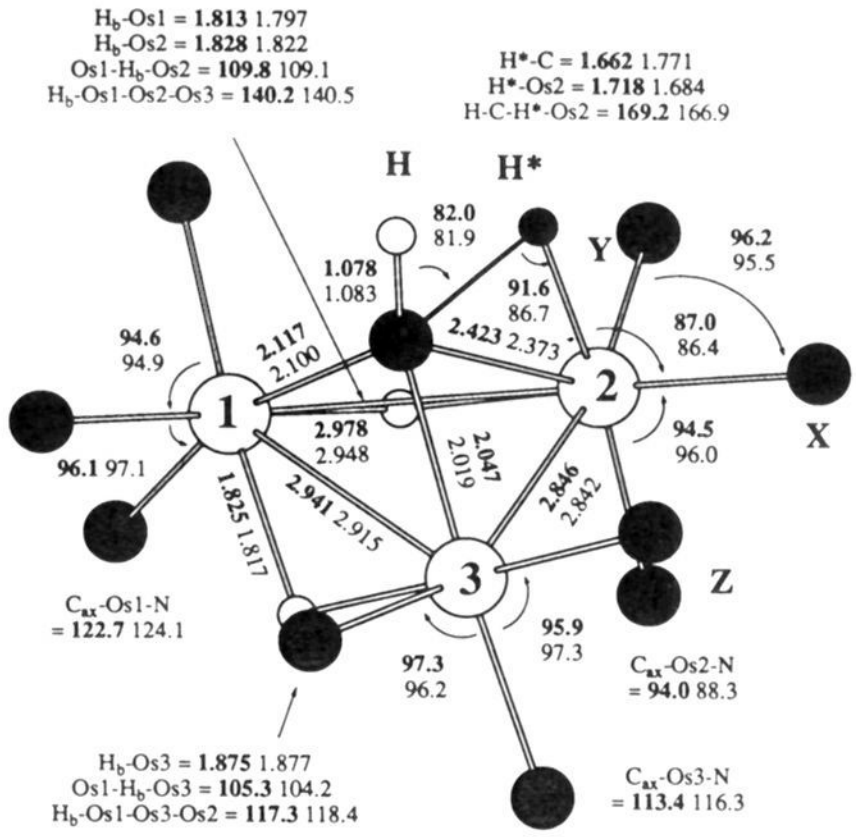

TS VI (C_1)

Figure 7. RHF optimized structure of the transition state **VI** between **V** and **VII** for H insertion into Os–C for Os (bold) and Ru (light). Distances are given in angstroms and angles in degrees. N is the center of the metal triangle.

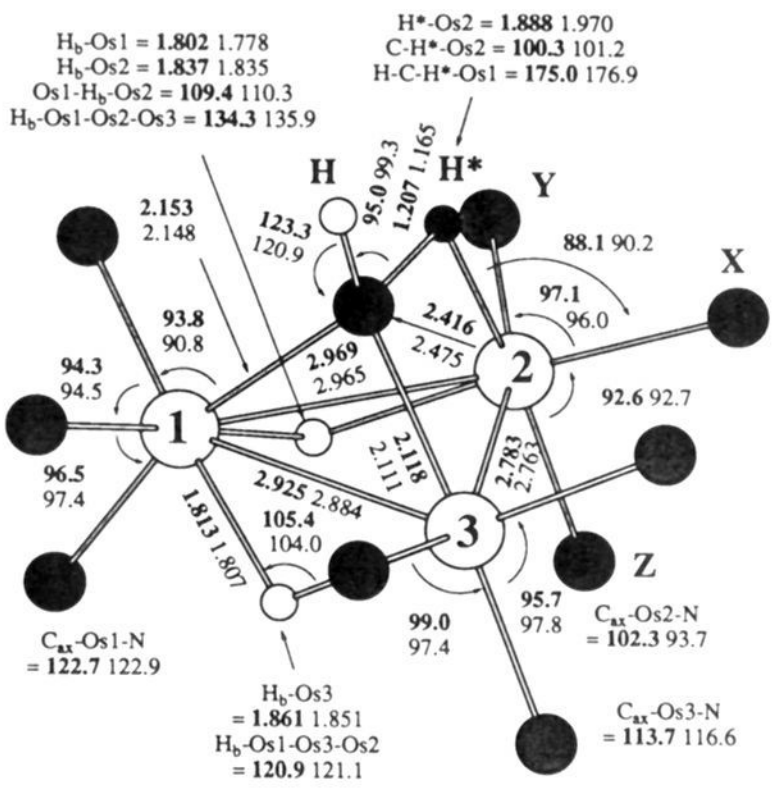

VII (C_1)

Figure 8. RHF optimized structure of the intermediate **VII** for Os (bold) and Ru (light). Distances are given in angstroms and angles in degrees. N is the center of the metal triangle.

toward the $HCOs^2$ plane, as indicated by the Os^2–H*–C–H dihedral angle of 169.2°. The Os^2–H* distance of 1.718 Å is much closer to 1.690 Å of reactant **V** than 1.888 Å of product **VII** of this step. The C–H* distance of 1.662 Å (vs 2.314 Å in **V**) is much longer than 1.207 Å in the product **VII**. These suggest that **VI** is a relatively early transition state. The C–Os^2 separation becomes slightly larger (2.423 Å) than 2.294 Å of **V**. The structure is similar to the transition states for reductive elimination/oxidative addition and therefore is regarded as the TS for reductive elimination of CH and H* from Os^2, where 4+ Os^2 (d^4) is reduced to 2+ Os^2 (d^6). The Os^2–Os^3 distance has become substantially shorter (2.846 Å) than 2.969 Å in **V**, leading to the much shorter

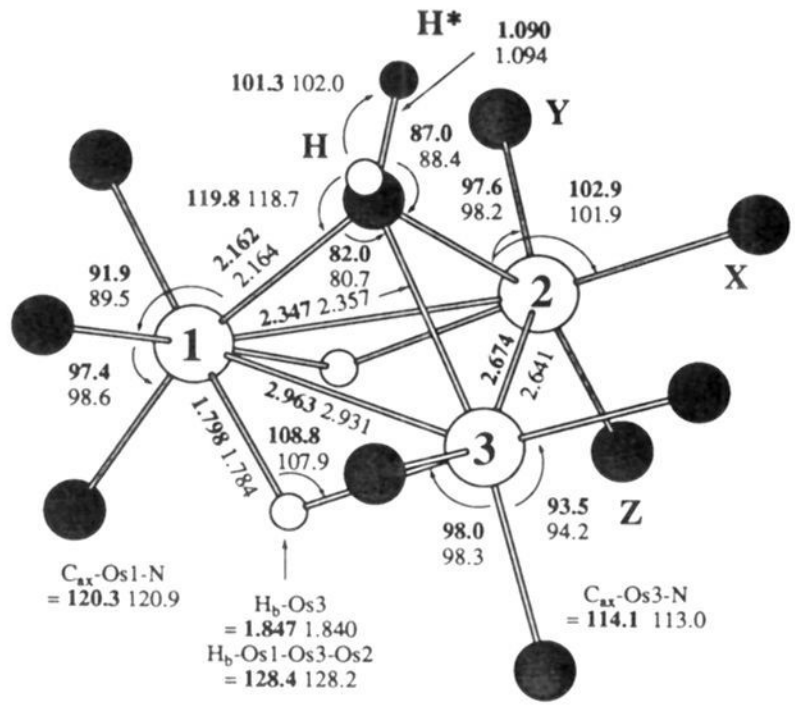

TS VIII (C_s)

Figure 9. RHF optimized structure of the transition state **VIII** between **VII** and **VII′** for H and H* exchange for Os (bold) and Ru (light). Distances are given in angstroms and angles in degrees. N is the center of the metal triangle.

distance in **VII**. Finally, one can see in Figure 7 that the $Os^2(CO)_3$ unit has already started to readopt the hexacoordination arrangement, increasing the C_{ax}–Os^2–N angle to 94.0°.

The stable intermediate **VII** is characterized by an Os–H–C bridge and by a very short Os^2–Os^3 bond of 2.783 Å vs 2.952 Å in **I**. Considering this step as reductive elimination, one can notice that the vacant coordination site appears on Os^2 and the new CH* bond is formed. Accordingly, the agostic interaction between them can take place to realize the Os–H*–C bridge. In the Os–H–C bridge, compared with the Os–H–Os bridge, the base Os–C bond distance is shorter than the Os–Os distance, and therefore the cyclic strain puts the bridged H further away from the base bond, with the Os–H distance of 1.888 Å, which is larger than 1.839 Å in **I**, and with the Os–H–C angle of 100.3°, which is smaller than the Os–H–Os angle of 106.9° in **I**.

Transition State VIII. For a degenerate reaction, i.e., the reaction where the reactant and the product are the same compound, at the middle point of the pathway, the optimized structure (an intermediate or a transition state) has to have the atoms being exchanged occupy symmetrically equivalent positions, or reflected by a symmetry operation.[26] Optimized under the C_s constraint, the structure **VIII**, shown in Figure 9, has the exchanging hydrides symmetrically equivalent and is a local minimum within this symmetry.

In order to identify the nature of this structure, we have diagonalized an approximate Hessian matrix, consisting of intrafragment and interfragment coupling elements obtained by numerically differentiating the gradient for the internal coordinates of the CHH* fragment and of estimated values obtained in the optimization for the other degrees of freedom. This approximate Hessian gave only one negative eigenvalue, which is in a″ irreducible representation, demonstrating that structure **VIII** is a transition state. Following the IRC, we actually could reach **VII**, establishing that **VIII** is the TS connecting the two enantiomers **VII** and **VII′**, as shown in Scheme 2. The content of the eigenvector associated with the negative eigenvalue shows that, at least in the vicinity of TS **VIII**, the reaction takes place to both directions through a tilt of the CH_2 group within its

(26) Mebel, A. M.; Morokuma, K.; Musaev, D. G. *J. Am. Chem. Soc.* In press.

(27) The largest off-diagonal matrix element between δ's and others was around 0.0005 au, which is much smaller than the smallest diagonal term of around 0.08 au.

Chart 1

	Os-Os distance/Å	
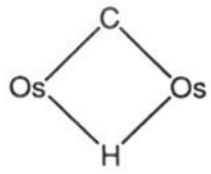	2.925-2.999	
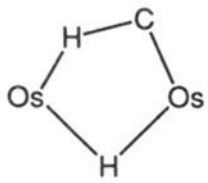	2.957	**XII**
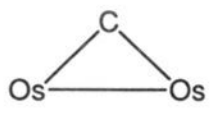	2.776	**XII**
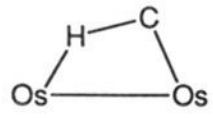	2.783	**VII**
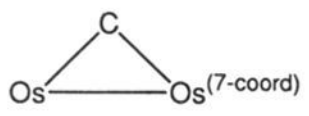	2.935-2.979	**III, V, X**
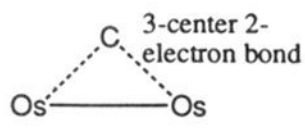	2.674	**TS VIII**

symmetry plane rather than through a rotation around the vertical axis. The calculation also shows that the coupling between the H and H* coordinates and the dihedral angle C–N–Os^1–Os^2, i.e., the motion of C out of the mirror plane, is quite important; a diagonalization of the Hessian in which only the matrix elements associated with the six coordinates of H and H* are numerically calculated gave only positive eigenvalues.

This structure, as shown in Figure 9, can reasonably be called a "CH_2" complex, though it is not an intermediate but a transition state; the C–H distance of 1.090 Å and the H–C–H angle of 101.3° are not far from those of free CH_2. This structure is also characterized by a very short Os^2–Os^3 distance of 2.674 Å vs 2.783 Å in **VII** and 2.952 Å in **I**, which will be discussed later. The Os^2–C–Os^3 bond is a three-center two-electron bond as shown in **6**. Therefore, the Os^2–C and Os^3–C bonds of 2.347 Å are weaker and thus longer by about 0.2Å than the Os^1–C bond.

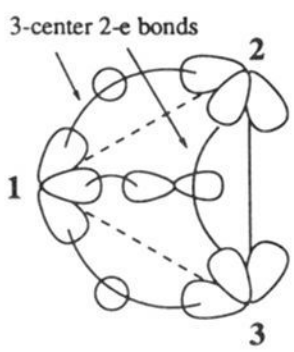

6

Os–Os Bond Distance. In this subsection, we discuss the Os–Os distances calculated in a variety of environments and summarized in Chart 1. It can be seen clearly that without a direct Os–Os bond, the Os–Os distance is longer than 2.9 Å, regardless of whether one of the bridging ligands is a C atom or a CH σ bond. However, a direct Os–Os bond replaces the Os–H–Os bond, and the Os–Os distance is decreased to about 2.78 Å as seen in **VII** and **XII**; the direct bond with a bridge makes

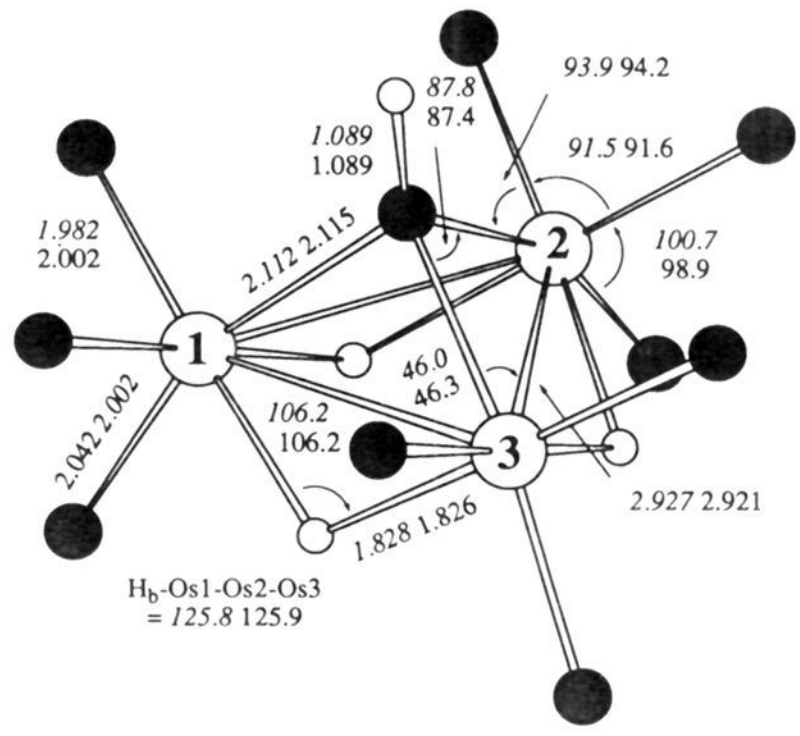

Reactant I (C_{3v} assumed)

Figure 10. RHF optimized structure of the reactant **I** for Ru. In italics are the preliminary fully optimized geometry values. Distances are given in angstroms and angles in degrees. N is the center of the metal triangle.

the Os–Os bond short. If the bridging bond is a sort of three-center two-electron bond as in TS **VIII**, the Os–Os distance decreases even more. In this case, the orbital of C is directed toward the midpoint between two Os atoms, and therefore the short Os–Os distance is favorable. In **III**, **V**, and **X**, one of the Os atoms is seven-coordinated, and the Os–Os distance remains longer than 2.9 Å, presumably because of the congestion, though they formally have a direct Os–Os bond.

(II) The $Ru_3(CO)_9(\mu\text{-}H)_3(\mu_3\text{-}CH)$ Complex. According to the experimental results, the behaviors of the Os and Ru compounds are similar, with an activation energy for the exchange reaction 3–5 kcal/mol lower for Ru than that for Os. One can thus reasonably envisage for the Ru complex a similar shape of exchange PES, i.e., the same mechanism as for the Os analog. Actually, we were able to locate for the Ru complex the same intermediates and transition states we obtained for the Os analog. The RHF optimized structures of **I** and **II**–**XIII** are shown in Figure 10 and Figures 3–9, respectively, and the energetics are shown in Table 1 and Figure 1.

A. Intermediate and Transition Structures. At first, we fully optimized the geometry of the reactant under the C_{3v} symmetry as shown in Figure 10. There are no experimental data for this compound for a direct comparison. A comparison with the structurally characterized isomorphous complexes $Ru_3(CO)_9(\mu\text{-}H)_3(\mu_3\text{-}CCl)$[28a] and $Ru_3(CO)_9(\mu\text{-}H)_3(\mu_3\text{-}CCH_3)$[28b] shows the same trend as found for the Os analog: the calculated distances are overestimated. The calculated Ru–Ru distance is 2.927 Å vs 2.8525(5) and 2.842(6) Å experimentally in the μ_3-CCl and μ_3-CCH_3 compounds, respectively. The calculated Ru–C_{ax} and Ru–C_{eq} distances are 2.042 and 1.982 Å, respectively, vs 1.995(2) and 1.914(2) Å for the μ_3-CCl complex and 1.956(19) and 1.869(15) Å for the μ_3-CCH_3 compound, and the Ru–C bond length is 2.112 Å calculated vs 2.063(2) and 2.083(11) Å in the μ_3-CCl and μ_3-CCH_3 complexes, respectively. Sheldrick et al. proposed NMR estimated Ru–H and H–Ru–H parameters of 1.81 Å and 103°, which are consistent with our calculations. Though one could resort to a C substituent effect, the relative error is larger for Ru than for Os, possibly illustrating a larger role of electron correlation in a second row transition metal. The calculated Ru–H distance of 1.828 Å is accurate enough, however,

(28) (a) Zhu, N. J.; Lecomte, C.; Coppens, P.; Keister, J. B. *Acta Crystallogr.* **1982**, *B38*, 1286. (b) Sheldrick, G. M.; Yesinowski, J. P. *J. Chem. Soc., Dalton Trans.* **1975**, 873.

to allow use of the RHF optimization for the determination of reaction pathways involving a hydride.

One can see in Figures 3–9 that Os and Ru structures are very similar. Distances and angles are usually equivalent within 0.02 Å and 3–4°, respectively, suggesting a similar behavior of the two metals.

B. Exchange Potential Energy Surface. Having similar structures for the Os and Ru compounds, we obtain qualitatively similar potential energy profiles for the exchange reaction, as seen in Figure 1. At the more reliable MP2 level, at the first step of the reaction, the outer pathway is more facile than the inner pathway, with the barrier of 18 kcal/mol for the former at TS **IX**, which is lower by 3 kcal/mol than the barrier 21 kcal/mol of the latter at TS **II**. At the second step, TS **XI** is slightly more stable than intermediate **X** at the MP2 level, suggesting that in the outer path, the first step, H* migration and turnstile rotation, and the second step, a further turnstile rotation, may take place without intermediate in one concerted step. On the other hand, the inner path requires the small activation energy of 4 kcal/mol.

The third and fourth steps of the reaction are also merged into one concerted step, since the MP2 energy of TS **VI** is lower than that of intermediate **VII**, making **VII** a sort of "inflection point" on the PES and combining these two steps as one. The MP2 activation energy relative to intermediate V is 17 kcal/mol, slightly smaller than that for the first step, indicating that the rate-determining step is the first step, as for the reaction of the Os complex. Overall, the hydride exchange reaction for the Ru compound has a rate-determining barrier of 18 kcal/mol, which is lower by 4 kcal/mol than that of 22 kcal/mol for the Os analog. Experimentally found are $\Delta G^{\ddagger} = 20.6$ kcal/mol at 34 °C for the Ru complex and $\Delta H^{\ddagger} = 24.0 \pm 1.7$ kcal/mol with a small entropy factor for the Os analog, with the former reaction having 3–5 kcal/mol lower activation energy than the latter. The present energy difference of 4 kcal/mol between the two compounds is consistent with the experimental observations.

Conclusions

An *ab initio* molecular orbital study has been carried out for the potential energy surface of hydride exchange reaction in $M_3(CO)_9(\mu\text{-H})_3(\mu_3\text{-CH})$ (M = Os, Ru). Relevant intermediate and transition structures have been determined at the RHF level and their energies calculated at the MP2 level of theory. The reaction can proceed in two distinct pathways. The first half of the "inner" pathway involves four steps: (1) migration of a bridged hydride H* to the inner equatorial position of a metal center, making it seven-coordinated; (2) clockwise turnstile rotation of four ligands, three carbonyls and H*, around the seven-coordinated metal; (3) insertion of H* into the M–C(H) bond; and (4) exchange of H* and H via a symmetric transition state, which is followed by the second half, the reversal of steps 3, 2, and 1 above with the role of H* and H exchanged. The "outer" pathway involves the following steps: (1′) migration of a bridged hydride H* to the outer equatorial position of a metal center, making it seven-coordinated; (2′) anticlockwise turnstile rotation of three carbonyls and H* around the seven-coordinated metal; and finally a merger with step 3 of the "inner" pathway. Some of these steps seem to take place as a concerted single step. Both pathways are similar in energies and are competitive but cannot be distinguished experimentally because they give an identical product. The activation barrier for the Os compound is about 22 kcal/mol, in good agreement with the experimental value. The mechanism for the Ru compound is essentially the same, with an overall barrier which is lower by about 4 kcal/mol, which also is in good agreement with experimental observations. It is not likely that there is a low-energy pathway in which the migrating hydride H* directly inserts into the M–C(H) bond without going through a seven-coordinated intermediate.

Acknowledgment. The authors are grateful to Professor John R. Shapley and Dr. A. M. Mebel for stimulating discussions. A part of the numerical calculation was carried out at the Computer Center of IMS. J.F.R. acknowledges the Japan Society of Promotion of Science for his postdoctoral fellowship. The present research was in part supported by a Grant-in-Aid for Scientific Research in the Priority Area of "Theory of Chemical Reactions" from the Ministry of Education, Science and Culture of Japan.

Supplementary Material Available: Geometries of structures **IX–XIV** (7 pages). This material is contained in many libraries on microfiche, immediately follows this article in the microfilm version of the journal, and can be ordered from the ACS; see any current masthead page for ordering information.